Translation of mechanical strain to a scalable biomanufacturing process for acellular matrix production from full thickness porcine bladders

To cite this article: Ashley Ward *et al* 2021 *Biomed. Mater.* **16** 065023

IOP Publishing Biomed. Mater. 16 (2021) 065023 https://doi.org/10.1088/1748-605X/ac2ab8

Biomedical Materials

OPEN ACCESS

RECEIVED
2 June 2021

REVISED
21 September 2021

ACCEPTED FOR PUBLICATION
28 September 2021

PUBLISHED
15 October 2021

PAPER

Translation of mechanical strain to a scalable biomanufacturing process for acellular matrix production from full thickness porcine bladders

Ashley Ward[1], Debora Morgante[2], John Fisher[1], Eileen Ingham[3] and Jennifer Southgate[2,*]

[1] School of Mechanical Engineering, Institute of Medical and Biological Engineering, University of Leeds, Leeds LS2 9JT, United Kingdom
[2] Jack Birch Unit, Department of Biology, York Biomedical Research Institute, The University of York, York YO10 5DD, United Kingdom
[3] School of Biomedical Sciences, Institute of Medical and Biological Engineering, University of Leeds, Leeds LS2 9JT, United Kingdom
* Author to whom any correspondence should be addressed.

E-mail: j.southgate@york.ac.uk

Keywords: urinary bladder, acellular matrix, bioprocessing, biomechanics, mechanical strain, finite element modelling, 3D printing

Supplementary material for this article is available online

Abstract

Bladder acellular matrix has promising applications in urological and other reconstructive surgery as it represents a naturally compliant, non-immunogenic and highly tissue-integrative material. As the bladder fills and distends, the loosely-coiled bundles of collagen fibres in the wall become extended and orientate parallel to the lumen, resulting in a physical thinning of the muscular wall. This accommodating property can be exploited to achieve complete decellularisation of the full-thickness bladder wall by immersing the distended bladder through a series of hypotonic buffers, detergents and nucleases, but the process is empirical, idiosyncratic and does not lend itself to manufacturing scale up. In this study we have taken a mechanical engineering approach to determine the relationship between porcine bladder size and capacity, to define the biaxial deformation state of the tissue during decellularisation and to apply these principles to the design and testing of a scalable novel laser-printed flat-bed apparatus in order to achieve reproducible and full-thickness bladder tissue decellularisation. We demonstrate how the procedure can be applied reproducibly to fresh, frozen or twice-frozen bladders to render $8 \times 8\ cm^2$ patches of DNA-free acellular matrix suitable for surgical applications.

1. Introduction

The urinary bladder is a highly compliant organ with primary function relating to the cyclical storage and expelling of urine. This dynamic feature is reliant on the composition and organisation of major components of the bladder wall, particularly the detrusor smooth muscle and the sub-urothelial lamina propria [1]. The extracellular matrix of the bladder wall is composed primarily of collagen types I and III, with the latter conferring the majority of the bladder compliance as a result of its organisation as loosely coiled bundles in the lamina propria. The network of collagen type III fibres has been shown to change significantly in morphology as the bladder changes in size: un-distended, the fibres are loose and do not exhibit a specific orientation, but as the bladder fills and distends, the fibres form distinct and tight coils in an orientation parallel to that of the overlying uro-epithelium. These structural changes in response to increased bladder volume are accompanied by a reduction in the relative thickness of the entire bladder wall [2]. When the bladder is fully accommodated, all collagen fibres are elongated and aligned parallel to the surface of the lumen; this point corresponds to the transition point on the stress–strain curve of the tissue [2, 3].

Acellular matrices (ACMs) are prepared from biological tissues by solubilising and removing cellular content, including nucleic acids, to leave the extracellular matrix intact. By removing cellular content, this process renders tissue-specific scaffolds that have potential use in a wide range of applications, including clinical use in tissue and organ regeneration

[4–8]. ACMs are considered particularly well suited for homotypic (same tissue) applications due to their retention of the natural tissue architecture, including composition, biochemical and structural features [1, 5, 9], whilst the absence of immunoreactive host materials, especially DNA, offers the potential to use such materials in allogeneic and even xenobiotic settings [10, 11]. This opens interest in the scale up and commercial production of such biomaterials. In urology, there is an unmet clinical need for tissue-integrative biomaterials for use in surgical reconstructive procedures such as urinary bladder augmentation and urethral reconstruction.

Bladder wall is a thick and dense tissue, and therefore most researchers have resorted to split-thickness bladder tissues to achieve complete decellularisation, often by dissection or mechanical delamination of the tissue layers [12–15]. A process was previously developed whereby porcine acellular bladder matrix (PABM) was achieved by exposure of intact inflated ex vivo bladders to a sequence of decellularisation solutions [9]. This approach exploited the natural accommodating function of the bladder as, by applying biaxial strain to the bladder wall, it reduced the tissue thickness sufficiently for the decellularisation solutions to fully penetrate the tissue. By achieving complete decellularisation without major collagen fibre denaturation, the resultant ACM retained the unique physical properties of the bladder in relation to compliance coupled with natural physical strength. Further characterisation revealed Porcine Acellular Bladder Matrix (PABM) to have tissue-integrative properties in a human organ culture model [16] and in a porcine surgical model [17]. However, the batch method of distending individual whole bladders is incompatible with a scalable manufacturing process, particularly as variability in the size of bladders makes it difficult to control the degree of inflation necessary to achieve complete decellularisation.

The aim of this study was to develop a method to manipulate full-thickness bladder tissue to enable reproducible and efficient decellularisation in a manner compatible with a commercial manufacturing process. To achieve this, a mechanical engineering approach was taken to determine the relationship between porcine bladder size and capacity, to define the biaxial deformation state of the tissue during the decellularisation procedure and to apply these principles to the design and testing of a novel scalable flat-bed apparatus to achieve full-thickness bladder tissue decellularisation.

2. Methods

A schematic of the experimental approach is shown in figure 1.

2.1. Tissue processing

2.1.1. Tissue collection and storage

Porcine bladders with remnant urethral and ureteric stumps were sourced from a local abattoir (Alec Traves Ltd Escrick, York). These were taken from pigs of mixed strains, mixed gender, aged 20–26 weeks, which were from the regulated food supply chain. In preliminary studies reproducing the original method described by Bolland and colleagues, bladders were transported to the laboratory on ice in Transport Medium (HBSS containing 10 mM HEPES pH 7.4 and 20 KIU ml^{-1} aprotinin) [9]. In all subsequent work, pig bladders were collected directly into plastic bags for transport to the laboratory at ambient temperature. The effect of freezing bladders within 4 h of collection at −20 °C was tested, including single and double cycles of freeze-thawing in order to incorporate optional preparatory stages into the protocol. Unless stated otherwise, all steps took place at ambient temperature and stored frozen bladders were thawed completely at ambient temperature for 4 h before use. To limit adventitious infections of the PABM during processing, all tissue processing steps were carried out aseptically in a class II safety cabinet. Each bladder (fresh or thawed) was inspected and any extraneous tissue removed by dissection.

2.1.2. Measurement of bladders

The empty bladder tissue volume was determined by displacement of buffer (isotonic phosphate buffered saline (PBS) at ambient temperature) in a measuring cylinder. After weighing to determine the mass, each bladder was laid flat with its dorsal surface facing upwards. A ruler was placed next to the bladder and an image captured perpendicular to the dissection board at a distance of 30 cm. The width and elliptical length and apex-to-ureter length were determined from the captured images using ImageJ and these values were used to calculate the bladder area below the ureter. The width was calculated at the widest point of the bladder and the apex-to-ureter length was defined as the distance between the bladder apex and the midpoint of the ureters. The below-ureter-area was calculated by finding the area contained by the points on the perimeter of the bladder and points placed at the base of the ureters. The error of the below-ureter-area was calculated as the sum of the error associated with the placement of the points and the error associated with calculating the area using the trapezium rule, assuming the perimeter of the bladder was approximately ellipsoid. The initial thickness was calculated by dividing the tissue volume by twice the total bladder area, and the precision of the initial thickness was calculated by summing the respective relative errors of the tissue volume and bladder area.

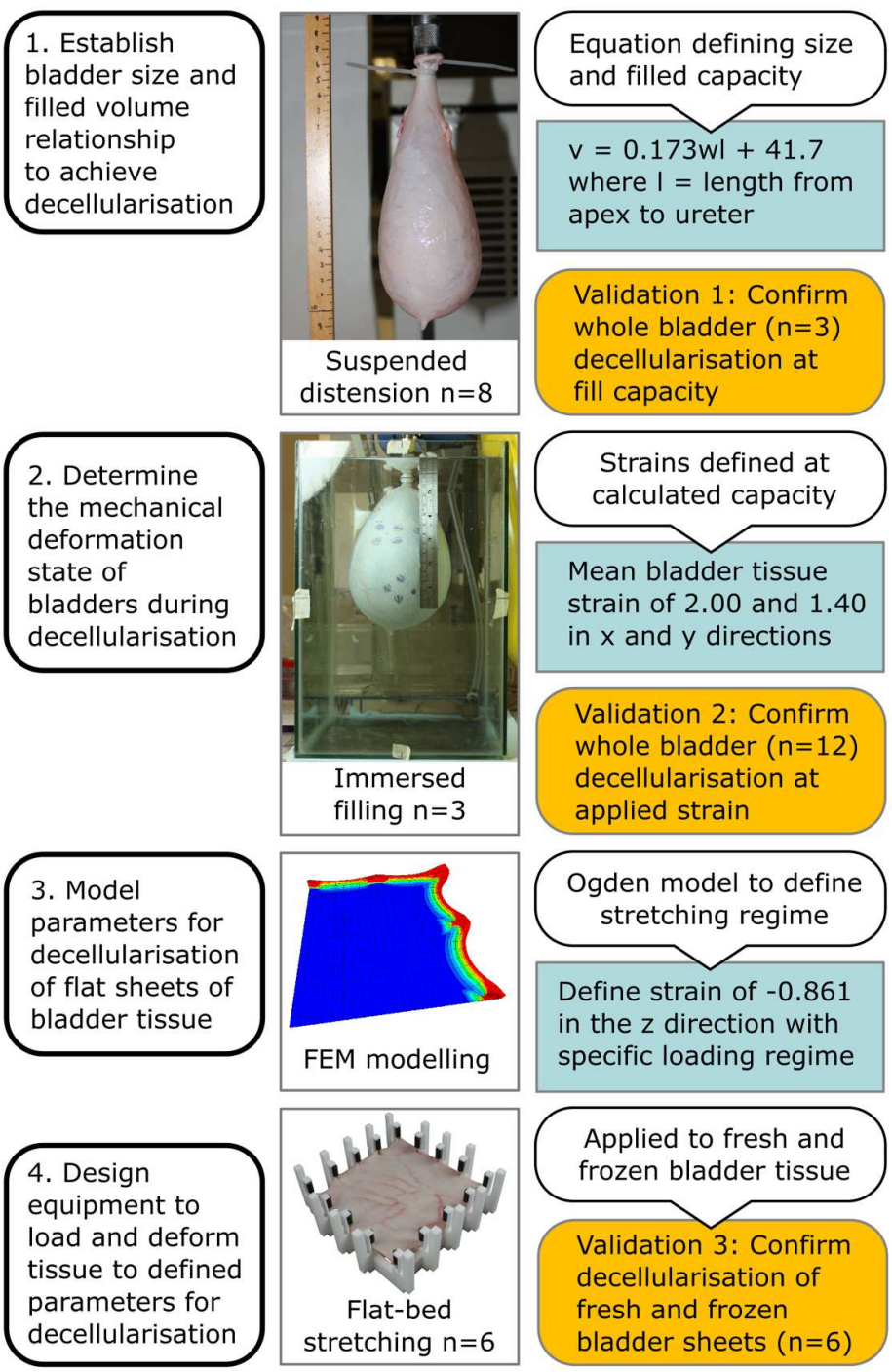

Figure 1. Schematic of the experimental approach. Each objective is represented in a subsection of the methods and results sections: Objective 1: sections 2.2 and 3.2; Objective 2: sections 2.3 and 3.3; Objective 3: sections 2.4 and 3.4; Objective 4: sections 2.5 and 3.5.

2.1.3. Dissecting intact or decellularised bladders to form a flat sheet

To dissect intact or decellularised bladders, the neck was cut off just below the ureters and discarded. An equivalent length cut was used to position and remove the bladder apex. A third longitudinal cut was made from neck to apex to open the bladder into a single-layered rectangular sheet. This approach of using three (rather than two) cuts allowed the tissue to lay in a low-stress flat sheet state from which samples of specific dimensions could be isolated by dissection.

2.2. Establish bladder size and filled volume relationship to achieve decellularisation (figure 1, Obj. 1.)

2.2.1. Determination of bladder capacity by suspended distension

To determine the relationship between bladder size and low pressure bladder capacity, intact bladders ($n = 8$) were held by the neck and allowed to hang freely during filling. To achieve filling, each bladder was connected via the urethra to a female filling tube secured with cable ties. The tube was held in a vice on a clamp stand fitted with a ruler so that the bladder was freely suspended. Bladders were distended slowly by placing 50 ml isotonic PBS into the funnel every 45 s, ensuring no trapped air. Any visible head of liquid was measured (error of ±2.5 mm) 30 s after each bladder filling, until either the height of the liquid was equal to the height of the neck of each bladder (capacity), or the weight of the filled bladder caused it to detach from the tube fitting (bladder capacity not determined). The equipment setup is illustrated in supplementary figure 1 (available online at stacks.iop.org/BMM/16/065023/mmedia).

2.2.2. Bladder decellularisation using calculated volumes

Decellularisation was carried out at ambient temperature on intact filled bladders by sequential incubation through the series of decellularisation solutions, as described by Bolland [9]. Intact bladders ($n = 3$) were contained in 3 L covered pots and filled via a funnel inserted into the bladder neck. The volumes used to fill bladders with were calculated using a relationship between bladder size and capacity. The bladder necks were then closed and the bladders suspended in the remainder of the same solution, using a total volume of 2 l.

The decellularisation stages [9] included a rinse in PBS containing 0.1% w/v ethylene diamine tetraacetic acid and aprotinin (10 KIU ml^{-1}) to inhibit protease activity; 24 h at 4 °C in hypotonic 10 mM Tris buffer (pH 8.0); 24 h in 0.1% (w/v) sodium dodecyl sulphate in 10 mM Tris buffer pH 8.0; a rinse, then 24 h in 1 unit ml^{-1} Benzonase (Novagen-Merck) to remove DNA. Bladder matrices were disinfected in 0.1% (v/v) peracetic acid in PBS for 3 h, washed in sterile PBS for 24 h, then 3 × 1 h, before storage in sterile PBS at 4 °C. Following any handling, matrices were re-disinfected in 0.1% (v/v) peracetic acid.

2.3. Determine the mechanical deformation state of bladders during decellularisation (figure 1, Obj. 2.)

2.3.1. Mechanical properties during immersed distension

This was carried out to determine the state of mechanical deformation of bladders during decellularisation. Fresh bladders were collected and prepared as above ($n = 12$). Additional bladders were collected and subjected to one ($n = 6$) or two ($n = 6$) freeze-thaw cycles prior to testing. Bladders were laid flat with their dorsal surface facing upwards and four 2 mm spots of haematoxylin were placed 5 mm from the midpoint of the widest section of the bladders in each direction along the longitudinal and axial axes as registration marks (figure 2(a)). The bladders were secured in a vice clamp (as above), before immersion in a tank of isotonic PBS, with bladders positioned such that markers were to the front, enabling images of the bladders and marks to be captured from the front, side and above (figures 2(b)–(d)). Bladders were distended by adding 50 ml PBS coloured with black food colouring over a period of 15 s, at repeat intervals of 60 s. During filling, the head of PBS in the tube was recorded (internal bladder pressure) at each time point. Images of the bladders and markers at each time point were also recorded in order to later calculate the stress and strain in the bladder wall during filling.

Details of the calibrations, image measurements and calculation of the variables describing the bladder deformation state during filling can be found in supplementary data 1.

Because the biaxial deformation of a material in each direction is dependent on the deformation in the other direction, it is not possible to calculate typical material properties directly from biaxial stress–strain curves. A variable (the uniaxial equivalent 'UE' strain) was therefore derived to allow modified stress–strain curves to be plotted in circumferential (x) and longitudinal (y) directions such that material properties could be calculated from stress–UE strain plots. The UE strain was derived from the stress–strain equations for an orthotropic material in plane (biaxial) stress, as shown in equation (1):

$$\varepsilon_{UE,x} = \frac{\varepsilon_x + \nu\varepsilon_y}{1+\nu^2}, \quad \varepsilon_{UE,y} = \frac{\varepsilon_y + \nu\varepsilon_x}{1+\nu^2}. \qquad (1)$$

The gradient of the curve derived from plotting stress against UE strain was used to derive the modulus of the material, as detailed in supplementary data 2. The x and y UE strains calculated for 12 fresh, 6 once- and 6 twice-frozen bladders plotted against the x and y stresses were used to derive the elastic moduli of the material (toe region and linear region moduli) in x and y directions. Storage condition (fresh, once- or twice-frozen) and direction (for x or y) were compared using a two-way ANOVA with Tukey honest significance difference post-test.

2.3.2. Decellularisation using controlled strain

Before decellularisation, haematoxylin markers were placed on the surface of the bladders as described above and the distance between the markers measured. Decellularisation was carried out as described previously, except that bladders ($n = 3$) were filled with volumes of solution required to

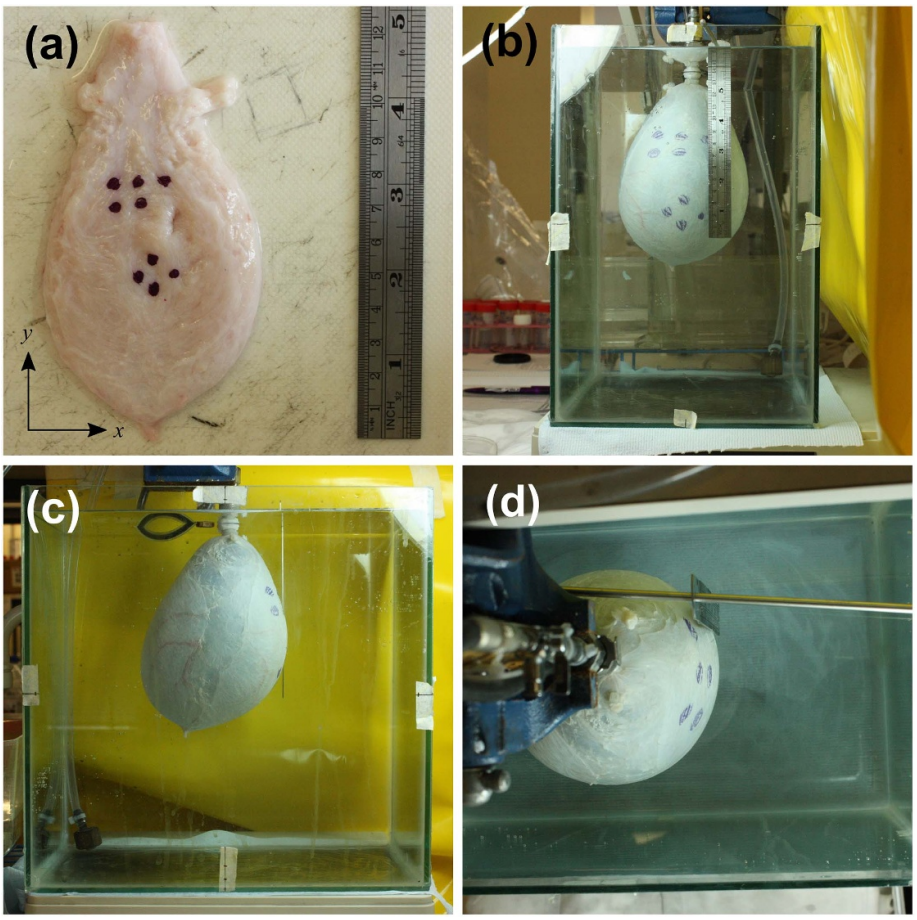

Figure 2. Images taken during the immersed distension experiment. A single pre-test image was taken before the start of each test (a). A front-angle (b), side-angle (c) and top-angle (d) image was taken at each time point during testing. These images were analysed using ImageJ and Matlab. The coordinate system used to analyse the bladders is shown in (a).

sufficiently stretch bladder walls (as indicated by the haematoxylin markers) to pre-defined strains.

2.4. Model parameters for decellularisaion of flat sheets of bladder tissue (figure 1, Obj. 3.)

Finite element modelling (FEM) was used to model the deformation of flat sheets of bladder material in order to find the optimal mode of stretching the tissue for effective decellularisation. By placing pins through the edges of flat sheets of bladder tissue, biaxial strain could be applied to the tissue by displacing the pins. However, deforming material in this way results in a heterogeneous state of deformation and in order to ensure the required deformation would be applied to the bladder tissue, the effects of variations in the number of pins and width of the pinned border were modelled using FEM.

A two-term Ogden model was used to model the bladder material in FEBio. The constitutive model parameters for bladder material were determined from the experimental data by using a least-squares approach to fit the model to the mean stress–strain curves for once-frozen and twice-frozen bladders, using the Matlab lsqcurvefit function. A Matlab script was written to automatically generate meshes of the bladder based on a number of input parameters which could be computed using FEBio and retrieved in Postview. The constitutive equation for the model and derived stress–strain relationship is given in supplementary data 3.

The measure used to assess the FEM of the bladder material was the strain of the material normal to the plane of the material. Specifically, the percentage of elements within 10% of this target z-strain was used. More detail is given on this in supplementary data 4. A mesh convergence study was performed to ensure an adequate mesh density was used.

To assess the effect of number of pins and border width on the z-strain of the material, FEBio was used to compute FEM models of flat sheets of bladder tissue with border widths varying from 2 to 20 mm (in 2 mm increments) and with a number of pins along each edge of the material from 3 to 9 (in unit increments). For each solution, the number of elements within 10% of the target strain was calculated and plotted against the number of pins and the border widths.

2.5. Design equipment to load and deform bladder tissue to defined parameters for decellularisation (figure 1, Obj. 4.)

2.5.1. Design and testing of flat-bed frame for decellularisation of bladder tissue sheets

A design specification for a scalable manufacturing process for decellularising bladders was drawn up (supplementary data 5). Based upon this, a design concept (flat-bed frame) was developed. The frame was designed using SolidWorks software to generate a CAD model of the design. The frames ($n = 3$) were 3D printed using the selective laser sintering method with Durafoam PA as the additive material (Keyworth Rapid Manufacturing Limited, Leeds, UK).

2.5.2. Decellularisaion of flat bladder sheets

Bladders were collected and prepared as above, and before the decellularisation procedure was performed bladders were either fresh ($n = 3$) or twice-frozen then thawed ($n = 3$). Before decelluarisation, bladders were dissected to form a flat sheet (as above) and each mounted onto a flat-bed frame. The procedure is described in figure 7. Decellularisation was performed as described above by submerging completely in the same series of decellularisation solutions, using the same volumes.

2.6. Histology and quantification of DNA content of decellularised tissue

Samples, approximately 1 cm^2 in area, were taken for histological analysis from all decellularised porcine bladder tissues. Before samples were taken the tissues were dissected to form flat sheets as described above. As a control, 1 cm^2 pieces were taken from the centre of the dorsal surface and the right lateral side of each of three non-decellularised bladders. Samples were fixed in 10% (v/v) neutral buffered formalin before routine processing and embedding into paraffin wax. Tissue sections of 5 µm were stained either with haematoxylin and eosin or with 0.1 mg ml^{-1} DAPI (4′,6-diamidino-2-phenylindole dihydrochloride; Sigma) to visualise double-stranded DNA. Sections were viewed using a Zeiss AX10 microscope using bright field or fluorescent microscopy with a DAPI filter. Images were captured using ZEN microscope software running on a desktop computer.

DNA was analysed using the DNeasy kit (Quiagen), according to the manufacturer's instructions. Briefly, samples from fresh and decellularised bladders were lyophilised and a known dry weight and digested using proteinase K. Samples were buffered to promote specific adsorption of DNA onto the silica-based membranes, before elution and quantification of total DNA at 260 nm using a NanoDrop™ ND-1000 spectrophotometer. Data is expressed as ng DNA per mg dry weight of tissue.

3. Results

3.1. Initial reproduction of intact bladder decellularisation by inflation protocol

Preliminary decellularisation experiments, conducted according to [9] on intact bladders inflated with 500 ml of solutions, demonstrated that the original protocol was not consistent for rendering larger bladders completely acellular (results not shown). These results indicated that larger bladders required filling with greater volumes of liquid to distend the bladder walls to the transition point and achieve adequate biaxial strain for complete decellularisation. A relationship was sought between bladder external dimensions in relaxed and filled low pressure capacity states, in order to calculate the inflated volume parameter predicted to be associated with effective decellularisation.

3.2. Establish bladder size and filled volume relationship to achieve decellularisation

Eight bladders were used to determine the natural bladder capacity when freely suspended. Capacity measurements were obtained from six bladders, whilst a further two bladders failed by becoming detached before reaching capacity, resulting in no data. Using bladder capacity ($n = 6$) as the variable, simple regression relationships were found between bladder capacity and elliptical length, width, width × elliptical length and tissue volume. An initial relationship between bladder capacity and width × elliptical length was found where $R^2 = 0.888$. This relationship was defined by equation (2), where v_c is capacity, w is width and l_e is elliptical length:

$$v_c = 0.143\, w\, l_e + 78.8. \quad (2)$$

To verify that this relationship between bladder dimensions and capacity resulted in effective bladder decellularisation, three bladders (width × elliptical length of 55 × 73, 61 × 72 and 62 × 84 mm) were decellularised by inflation to the respective calculated capacity volumes of 653, 707 and 824 ml. This represented a mean increase of 46% over the volume used in the original procedure [9] in which a set volume of 500 ml was used. These three bladders all produced matrices shown to be free of cellular material upon histological analysis and with >98% of DNA removed relative to the native tissue (4370 ± 1930 vs 45.7 ± 68.8 for fresh versus decellularised tissue, where values represent mean DNA ng mg^{-1} dry weight ± 95% CI).

In subsequent studies, a more accurate measure of bladder size was employed using the apex-to-ureter length and this was used to determine the relationship with bladder capacity (supplementary figure 2). This resulted in a stronger relationship between bladder

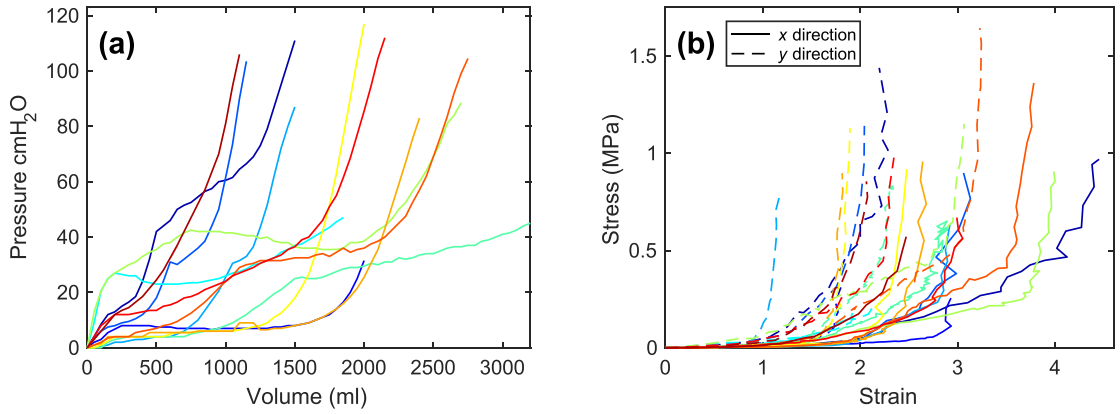

Figure 3. Pressure-volume (a) and stress–strain (b) curves of fresh bladders tested by immersed distension. Each colour represents a single bladder.

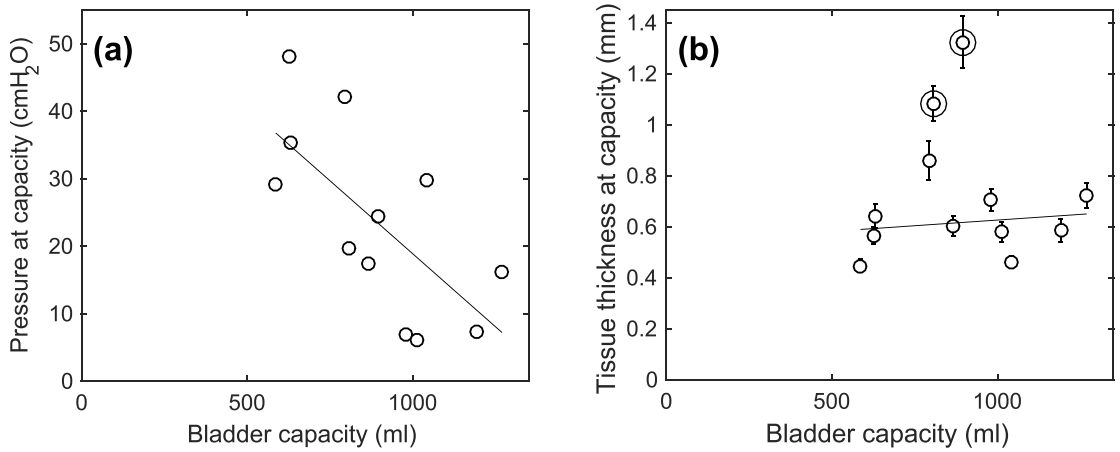

Figure 4. Material variables of fresh bladders filled to their calculated capacities. When filled to capacity, an increase in capacity indicates a decrease in pressure (a), whereas tissue thickness is invariant with bladder capacity (b). Each point represents a single bladder. Measurement errors (SEM) are shown. Outliers are indicated with a circle around the points.

capacity and the width x apex-to-ureter length ($R^2 = 0.924$), as defined by equation (3), where l_a is the length from apex to ureter:

$$v_c = 0.173\, w\, l_a + 41.7. \quad (3)$$

Twice frozen bladders ($n = 3$) were decellularised by inflation to the calculated capacity volumes determined by the revised relationship (width × apex to ureter length) of 680, 722, 772 ml; a mean volume increase of 45% compared to the original process. These bladders all produced matrices shown to be free of cellular material by histology and a DNA content reduction of over 99% (mean ± 95% CI for fresh vs twice-thawed decellularised tissue = 2580 ± 1090 vs 13.1 ± 9.4 ng mg^{-1} dry weight; $n = 3$ per group).

3.3. Determine the mechanical deformation state of bladders during immersed decellularisation

3.3.1. Immersed distension to determine the deformation (strain) of bladders at calculated capacity

The mass and tissue volume of bladders showed a very strong relationship ($R^2 = 0.997$; $n = 20$) and indicated bladder tissue had a specific mass of 1010 m^3 kg^{-1}, equivalent to a density of 990 kg m^{-3}. Filling of intact bladders showed an initial pressure rise, followed by a period of low-pressure filling and finally a steep rise in pressure as maximum capacity was approached. The stress–strain curves showed an initial phase of low-stress elongation (the toe region), followed by a transition into a phase of steep rise in stress (the linear region). The pressure vs volume and stress/strain relationships using fresh bladders are illustrated in figure 3.

The majority of fresh bladders failed by bursting. The stress, strain, pressure and bladder thickness at the point of calculated filled capacity was taken to describe the deformation state of the bladder (figure 4). There was a weak negative correlation between pressure and capacity ($R^2 = 0.470$; $p = 0.014$), but all other relationships tested were insignificant. Importantly, this confirmed that the strain of the bladder tissue was invariant with capacity (p values of 0.331 and 0.667 in the circumferential (x) and longitudinal (y) directions respectively)

and the means of the strains in the x and y directions were determined to be 2.00 and 1.40.

3.3.2. Decellularisation under controlled strain

Three bladders were decellularised by immersing them in decellularisation solutions and using a peristaltic pump to fill them to apply the calculated mean strains of 2.0 and 1.4 in the x and y directions (as indicated from the registration marks). However, the ratios of the x strain to y strain in the tissue (as indicated by the markers) were not equal to exactly 2.0:1.4. If the x strain of the tissue was increased to 2.0, the y strain was either less than or greater than 1.4, depending on the bladder. To overcome this problem, bladders were stretched by filling until the strains had reached a minimum of 2.0 in the x direction and a minimum of 1.4 in the y direction. This resulted in measured x and y strains of 2.0 and 1.8; 2.0 and 2.7; and 2.6 and 1.4 for the three bladders, respectively. Applying the decellularisation protocol resulted in complete removal of all cellular and nuclear material; as confirmed by histology, staining sections with DAPI and analysis of total DNA content (fresh 3970 ± 272 vs decellularised 16.1 ± 39.2 ng mg^{-1} dry weight $\pm$ 95% CI). This validated that the strains found in bladder walls filled to capacity were compatible with successful decellularisation.

Examination of the distance between the registration markers before and after decellularisation revealed that the bladders did not contract back to their original size before decellularisation. The means of the final strains in the x and y directions were 0.926 and 0.488 respectively, relative to the pre-decellularisation measurements. This was likely due to the relaxation of the collagen matrix in all three bladders tested. In order to predict the final strain from decellularisation strain, linear regression was performed with decellularisation strain as the predictor variable and final strain as the response variable; this equated to a relationship between final and decellularisation strains of $y = 0.730x - 0.534$ ($R^2 = 0.963$). This information was applied to calculate the initial size of tissue required to produce a decellularised patch of specific size.

3.3.3. Effect of freezing on material properties of bladder tissue

To determine whether freezing of bladder tissue for storage prior to processing affected the material properties of the tissue in terms of stress/strain relationships, bladders subjected to one ($n = 6$) or two ($n = 6$) freeze-thaw cycles were tested mechanically by immersed distension to derive the stress–strain curves as described for fresh bladders. No statistical difference was found between the toe region modulus and the transition stress of fresh, once-frozen and twice frozen bladders. There was a small but significant increase in the linear region modulus and transition stress of fresh bladders compared to the once- and twice-frozen bladders. No significant difference was found between once-frozen and twice-frozen bladders. This is shown in figure 5.

3.4. Model parameters for decellularisation of flat sheets of bladder tissue

It was considered that applying the required strains to bladder tissue in a flat sheet configuration would be compatible with a manufacturing process for PABM. To apply biaxial strain to the highly compliant material of the bladder wall, the material needed to be deformed from discrete points along the edges of the tissue. The stretching of flat sheets of bladder using this method was modelled using FEM to find an optimal stretching regime.

By placing pins through the edges of flat sheets of bladder tissue, biaxial strain could be applied to the tissue by displacing the pins. However, using this method results in a heterogeneous state of deformation of the material. To assess the extent of this variation, the effects of variations in the number of pins and width of the pinned border were modelled using FEM. To comply with anticipated surgical requirements, regions of the bladder tissue were modelled so that an 8 cm $\times$ 8 cm region of the bladder material was produced when biaxial strains of 2.0 and 1.4 were applied to the tissue (determined as described above).

The Ogden model was chosen to model the material deformation of the bladder (details provided in supplementary data 3). The model parameters were calculated from mean stress–strain biaxial test data, using the `lsqcurvefit` function in Matlab. Although the model considers the material to be isotropic, the flexibility of the model allowed the complex stress–strain response to be modelled. Positive strain applied to bladder tissue in the x and y directions results in negative strain in the z direction. The z-direction stretch was calculated for the case when the required strains of 2.0 and 1.4 were applied to an incompressible material in the x and y directions. This z stretch was equivalent to a strain in the z direction of $\epsilon_z = -0.861$ and a z Lagrange strain of $\epsilon_{Lz} = -0.490$ (for calculations see supplementary data 4). The criterion for successful bladder stretching was the number of elements which were stretched so that the z strain was within 10% of $\epsilon_{Lz} = -0.490$.

A Matlab script was written to automatically generate meshes of the bladder based on a number of input parameters which could be computed using FEBio. This allowed meshes with varying numbers of pins, border widths and mesh densities to be generated. A mesh convergence study was performed to determine the optimal mesh density. Numerous meshes were generated with pin numbers from 3 to 9 and border widths from 2 to 20 mm. The models demonstrated that deforming the tissue using five discrete points along each edge of the material would be adequate to ensure that the required strains

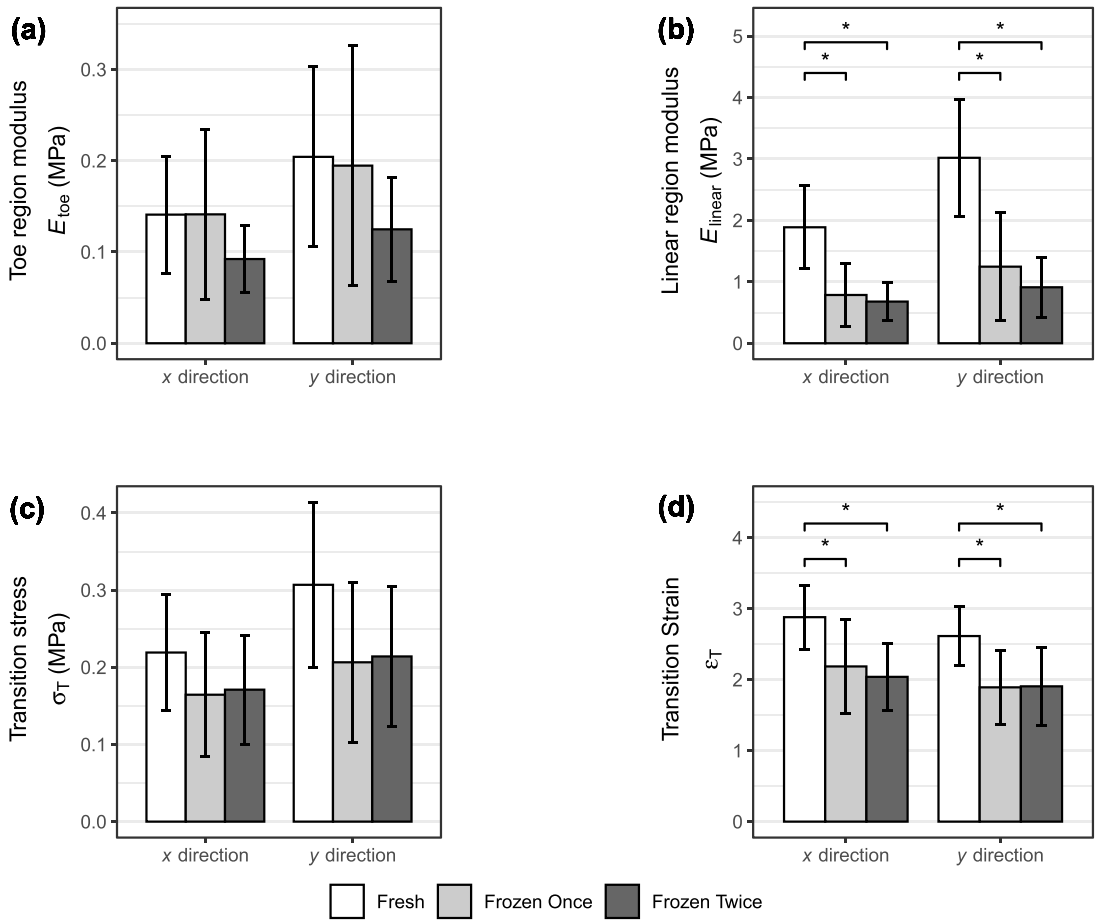

Figure 5. A comparison of stress/UE strain curve parameters of fresh, once-frozen and twice-frozen bladders. The parameters which were compared were toe region modulus (a), linear region modulus (b), transition stress (c) and transition strain (d). Bars represent the means of the parameters, and error bars represent the 95% confidence intervals. The differences between the means for each parameter were compared using a Tukey test, ignoring significant differences between the two directions. Significant differences between means ($p < 0.05$) are indicated with *.

would be applied to the tissue for decellularisation to occur.

The stretching of a full size sheet of bladder was then modelled which had a main area (bounded by the pins) of 47 mm × 60 mm. Over 99% of the elements in the central 80% of this area of tissue were stretched to within the required z strain range when an outside border of 2 mm or greater was used. Based upon the final strain of the bladder after decellularisation determined above, this central region would become approximately 8 cm × 8 cm square after decellularisation (figure 6).

3.5. Equipment design to load and deform tissue to defined parameters for decellularisation

Equipment was designed and produced to the design specifications (supplementary data 5) to enable dissected bladder sheets to be held in the state of deformation (defined above) required to achieve decellularisation. The equipment took the form of a 3D-printed frame and a procedure was developed using a guide plate (dimensions 47 mm by 60 mm, with 5 mm border) to dissect tissue to the required size and aid stretching of the bladder tissue sheet onto the frame (figure 7).

To test the flat bed decellularisation principle, six bladders (three fresh and three twice-frozen then thawed) were cut into flat sheets and stretched onto the frame. Bladders were placed into containers and decellularised by submerging in the sequential decellularisation solutions.

Stained histological sections of decellularised bladder samples demonstrated removal of cellular material and DNA (figures 8 and 9).

For DNA content, samples decellularised using the flat-bed method had a DNA content of $17.5 \pm 71.9\,\text{ng}\,\text{mg}^{-1}$ and $29.2 \pm 73.9\,\text{ng}\,\text{mg}^{-1}$ for fresh and twice-frozen bladders respectively (mean ± 95% CI). This corresponded to a mean reduction of 99.3% and 98.9% for fresh and twice-frozen bladders respectively relative to the native controls.

4. Discussion

A variety of different tissues have been reported to be successfully decellularised in the literature, such

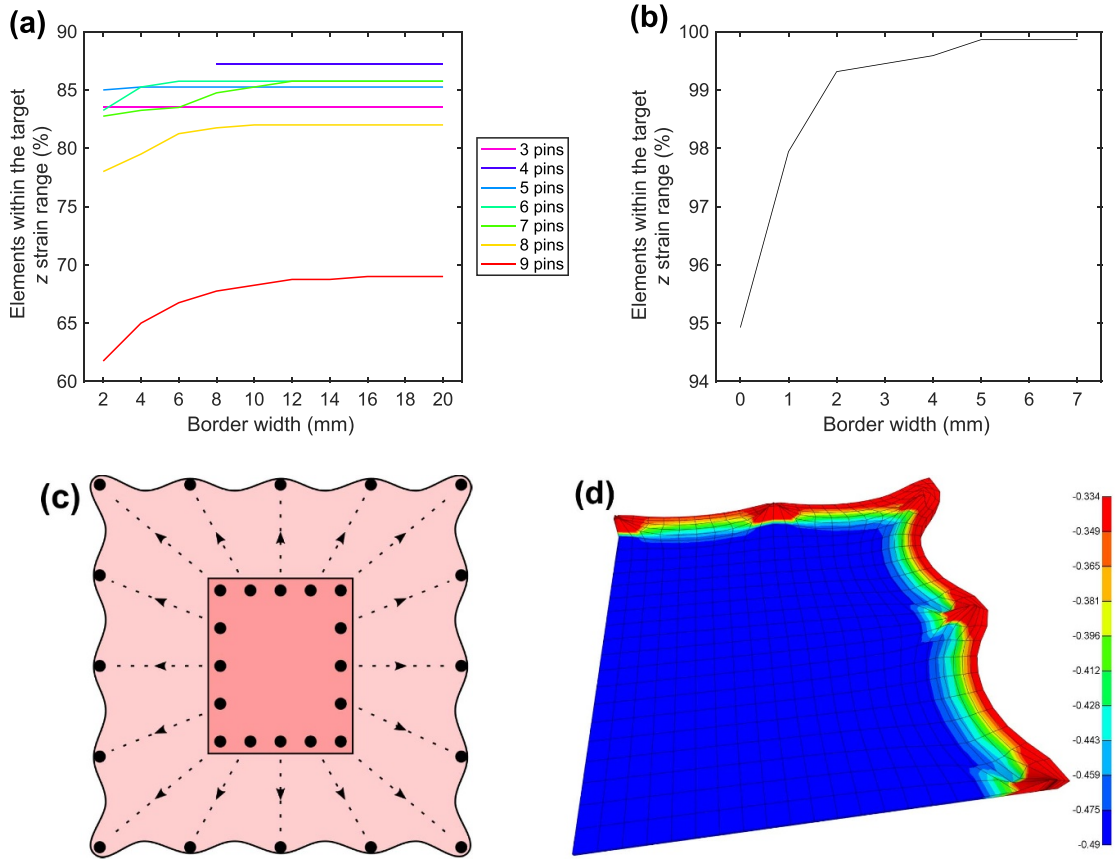

Figure 6. The effect of border width and pin count on the *z* strain of the elements in the modelled tissue (a). The effect of border width on the *z* strain of the elements in the central 80% of the modelled tissue, using 5 pins (b). A schematic of the tissue deformation which was modelled, demonstrated using 5 pins along each tissue edge (c). Visual output of a modelled deformation, demonstrating a 5-pin stretching regime. The colour gradient represents the *z* strain of the elements (d).

as porcine cardiac valves [18], porcine small intestine submucosa (SIS [19]), porcine aortic root [20], ovine forestomach matrix (OFM [21]) and porcine urinary bladder matrix (UBM [22]). The techniques used to decellularise these tissues typically involve combinations of physical and chemical processes in order to remove immunogenic material. The chemical processes rely on the diffusion of the chemicals (enzymes, detergent, etc) into the tissue for them to act on the cellular material. The diffusion of these chemicals is affected by time, temperature, concentration gradient, the permeability of the material, and the diffusion distance (tissue thickness) over which the chemicals must diffuse. The concentration of the solution and the incubation time of the tissue must both be limited to prevent excessive action on the tissue near the tissue/solution boundary. The incubation temperature is limited to the working temperature range of the solution, and must also be within a range which does not cause damage to the tissue (e.g. below the denaturation temperature of collagen). Material permeability is defined by the tissue and is not a controllable factor. Given these restrictions, there must therefore be a critical thickness of tissue above which a tissue is not able to be decellularised for a given decellularisation method.

The thickness of non-distended full-thickness porcine bladder wall is approximately 5 mm and when placed non-distended in decellularisation solutions with no liquid in the lumen, the effective thickness of the tissue is double this. In the literature, investigators working to decellularise other tissues including SIS, OFM and UBM have used physical delamination in order to isolate a particular layer of the tissue [21, 23, 24]. However, doing this may rob the ACM of its full architecture.

Previously a process was developed to decellularise porcine bladders [9]. To overcome the problem of bladder thickness, the method involved distending bladders by not only placing them in, but filling them with, decellularisation buffers. Distending the organs utilised the natural ability of bladders to contain large volumes during normal physiological function and resulted in the application of biaxial strain to the bladder walls. This caused the bladder walls to reduce in thickness, which allowed adequate diffusion of the decellularisation buffers throughout the tissue. This method of applying strain to the tissue during the decellularisation process works well for bladder tissue because it is highly compliant. Other tissues, which undergo lower physiological strains, are not likely to demonstrate a significant increase in decellularisation

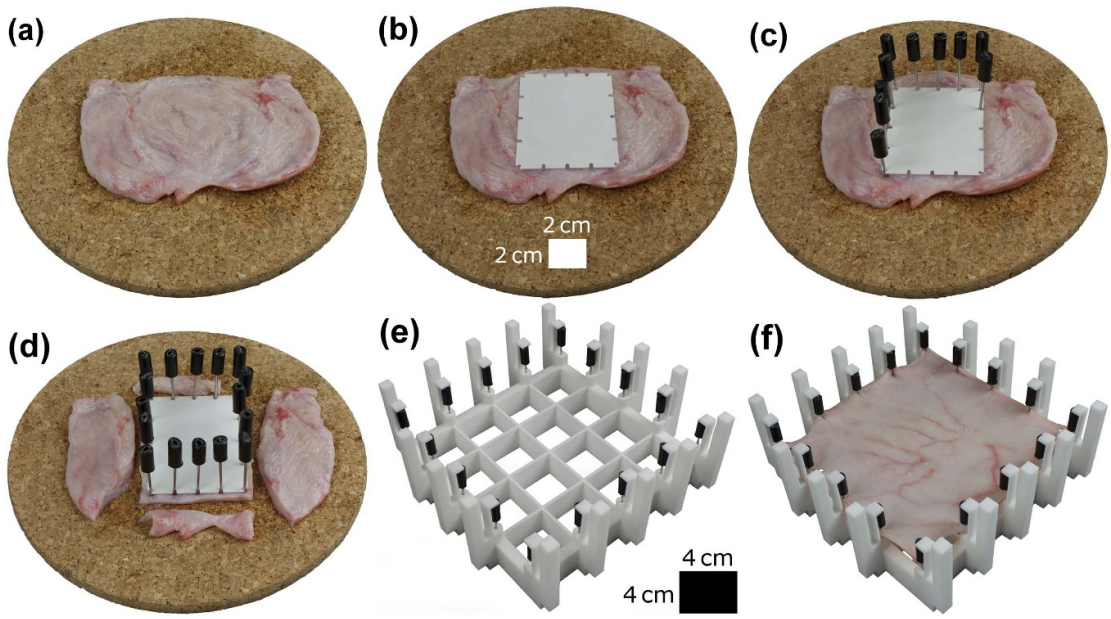

Figure 7. The procedure for stretching bladder tissue on to the frame. After dissecting into a flat sheet, the bladder was laid flat on a cork board, lumen side down (a). The pin guide plate was placed on the centre of the bladder (b). Notches on the guide plate were used to push pins through the required points on the bladder and into the cork board (c). With all the pins in place, excess bladder material was removed (d). The manufactured frame, shown before the tissue was mounted, with the pins in position (e). The guide plate was removed, then the pins were removed from the cork board. Care was taken to ensure that all pins remained in the tissue. The tissue was mounted manually by securing individual pins into position on the frame, stretching the tissue (f). Pins were mounted in opposing pairs to stretch the tissue evenly. The scale for (a)–(d) is shown on (b), and the scale for (e)–(f) is shown on (e).

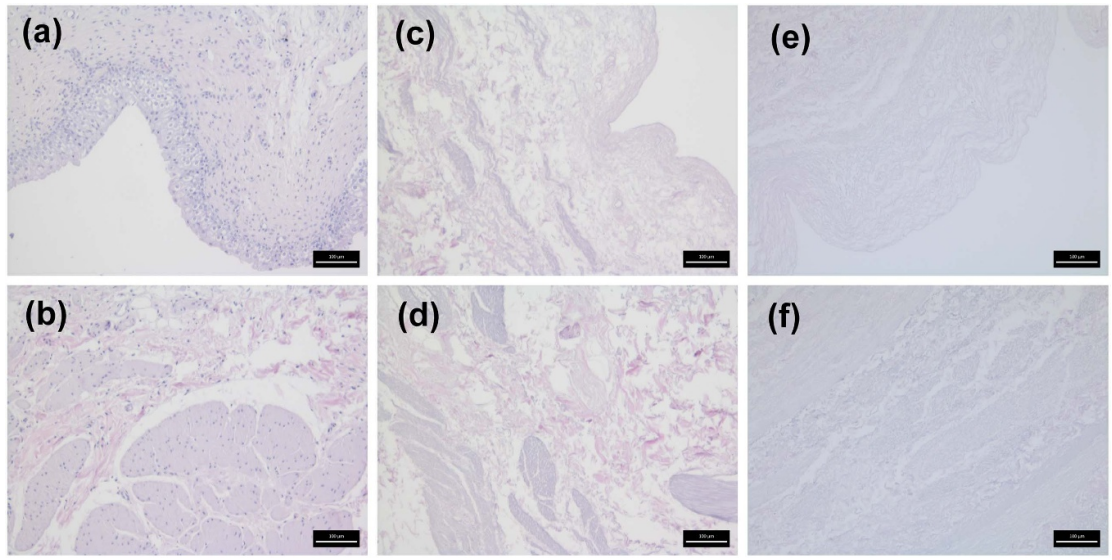

Figure 8. Images of H&E stained sections from bladders decellularised using the flat-bed method. (a) and (b) are fresh controls; (c) and (d) are from bladders decellularised from frozen; (e) and (f) are from bladders decellularised from fresh. (a), (c) and (e) are images of the luminal surface and (b), (d) and (f) are images of the muscular layer. Scale bars are 100 μm.

if a strain is applied during their decellularisation process. A similar method applied to a different tissue was unable to be found in the literature [25].

However, the method of distending the organs was not considered to be compatible with a manufacturing process. The main aim of this study was to develop a new method of deforming bladder tissue which would be compatible with a manufacturing process. To facilitate this, a relationship was found between the specific volumes that bladders of different sizes needed to be filled with during decellularisation to ensure complete cell removal. The filling volumes were then used to determine the state of deformation of bladders during decellularisation. It was found that the biaxial strain of the tissue was constant across all bladders filled to capacity.

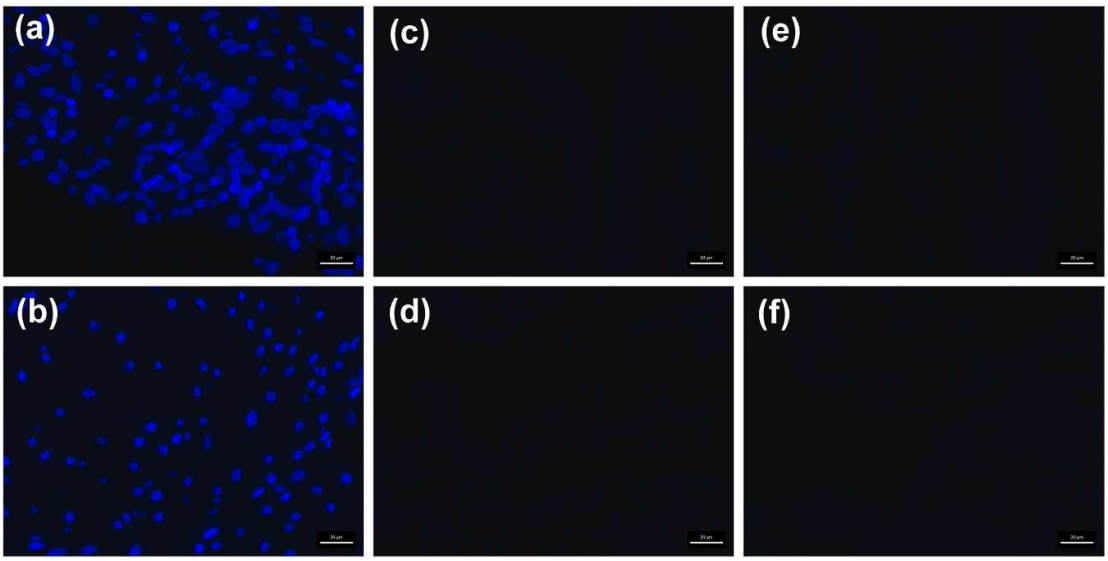

Figure 9. Images of DAPI stained sections of bladders decellularised using the at-bed method. (a) and (b) are fresh controls; (c) and (d) are from bladders decellularised from frozen; (e) and (f) are from bladders decellularised from fresh. (a), (c) and (e) are images of the luminal surface and (b), (d) and (f) are images of the muscular layer. All images were captured at 40 magnification and same exposure. Scale bars are 20 μm.

Decellularising bladder tissue in a flat sheet configuration was chosen, as it would be most suited to a manufacturing process. A suitable mode of stretching sheets of bladder tissue was determined by modelling the deformation of the tissue when the required strains of 2.0 and 1.4 in the x and y directions were applied. Strains of these magnitudes have been observed by other studies in the literature, in addition to demonstrating similar anisotropy [3]. This biaxial strain was applied to the tissue during decellularisation in order to mimic the strain the tissue would undergo during normal functioning, so that during decellularisation the strains applied would be physiologically anisotropic.

To apply these biaxial strains to the tissue, it was decided to apply the stretch using discrete points (e.g. hooks or pins). Cruciform-shaped specimens have also been used to apply biaxial strain to tissue [26], however these require much larger pieces of tissue to be used which would not have been possible given the size of porcine bladders. The method of applying biaxial strain using discrete points is one which has been commonly adopted in the literature [27–30]. Deforming tissue in this manner was also conducive to producing patches of the square 8 cm × 8 cm shape required clinically. However, this method of stretching did not result in application of a completely uniform strain field to the tissue, and therefore a mode of stretching was sought which would provide adequate strain to a piece of tissue of the required size. FEM was used to determine an optimal mode of stretching bladder tissue. The z strain of the tissue was used as the measure of tissue stretching efficacy. Specifically, the fraction of elements which were stretched to within 10% of the target z strain was calculated for each computed model, and used as the measure of comparison between different models. Stretching a piece of tissue using greater than five discrete points along each side of the rectangular material resulted in a negligible increase in the area of the tissue which was stretched to within the required specifications. An optimal number of five discrete points, when applied to stretching tissue biaxially, has also been reported elsewhere [31].

For a bioprocess which would be translatable to a large-scale manufacturing process, the tissue should be able to be frozen and thawed, ideally twice, to allow for feasible transportation and storage of the material. Other studies have shown that freezing can result in a significant change of the mechanical properties of other tissues [32]. However, freeze-thaw processing has been demonstrated as a viable method to assist in the decellularisation of some tissue [25]. To ensure that freeze-thaw cycles would not adversely affect the PABM, mechanical distension tests were performed on fresh, once- and twice-frozen bladder tissue. A significant difference in mechanical properties was observed between the fresh and frozen bladders, however this change was relatively small and strain was applied beyond that which would be required for decellularisation of the tissue.

We did not repeat extensive characterisation of the extracellular matrix in this study as this was described for fresh and decellularised bladder tissues previously, where the precise same strain and decellularisation protocol was applied to intact bladders [3, 9]. Here, using a novel process developed to enable manufacturing scale up, we selected key protocols incorporating histology, DAPI staining and DNA quantification

to demonstrate complete decellularisation. The results verified removal of cellular and nuclear materials, whilst preserving the physical characteristics of the underlying collagenous matrix to render a highly compliant, full thickness PABM. We have elsewhere demonstrated the potential for decellularised matrix produced conventionally from intact bladders to be used in urethral reconstructive surgery [17] and intend in future translational work to use full thickness PABM processed from flat sheets, as described here.

The frame which was designed to hold bladder tissue in a flat stretching regimen was a prototype suitable for a lab-based decellularisation process because it was both inert, autoclavable, and required human intervention to stretch the tissue. The current solution does not alone represent a commercially viable solution, but may be adapted and scaled-up to suit a commercial process. A mechanically-controlled method of stretching the bladder may provide more uniform stretching, due to the viscoelastic nature of the tissue.

5. Conclusions

In conclusion, this study demonstrated that applying suitable strains to flat sheets of bladder tissue was a viable method of deforming bladder tissue in order for it to be decellularised. Freezing the tissue up to two times before decellularisation resulted in some small but significant changes to the mechanical properties of the tissue, but did not affect the efficacy of the decellularisation process. It therefore may now be feasible to commercially produce decellularised full-thickness porcine bladder tissue, for such applications as hypospadias repair [17].

Data availability statement

All data that support the findings of this study are included within the article (and any supplementary files).

Acknowledgments

We thank Dan Thomas for excellent laboratory support.

This study was carried out as a PhD studentship awarded to Ashley Ward and funded by the EPSRC Centre for Doctoral Training in Tissue Engineering and Regenerative Medicine (Grant No. EP/L014823/1), with a CASE award from Tissue Regenix Group. Debora Morgante was registered as a PhD student with the Hull York Medical School and received funding from the Medical Technologies Innovation and Knowledge Centre (phase 2—Regenerative Devices) funded by the EPSRC under Grant No. EP/N00941X/1 as Proof of Concept award PoC045. The work leading to the development of PABM was originally funded by the Biotechnology and Biological Sciences Research Council (BBSRC) on Grant Nos. E-20352 and BB/E-527220/1. Jennifer Southgate receives programme funding from York Against Cancer.

Conflict of interest

Declaration of conflicting interests: The author(s) declared the following potential conflicts of interest with respect to the research, authorship, and/or publication of this article: John Fisher and Eileen Ingham are shareholders of Tissue Regenix Group PLC. The authors confirm that there are no other known conflicts of interest associated with this publication and there has been no significant financial support for this work that could have influenced its outcome.

ORCID iDs

Ashley Ward https://orcid.org/0000-0003-4434-5273
Debora Morgante https://orcid.org/0000-0001-7616-2274
Eileen Ingham https://orcid.org/0000-0002-9757-3045
Jennifer Southgate https://orcid.org/0000-0002-0135-480X

References

[1] Evren S, Loai Y, Antoon R, Islam S, Yeger H, Moore K, Wong K, Gorczynski R and Farhat W A 2010 *Cells Tissues Organs* **192** 250–61
[2] Chang S L, Howard P S, Koo H P and Macarak E J 1998 *Neurourol. Urodyn.* **17** 135–45
[3] Korossis S, Bolland F, Southgate J, Ingham E and Fisher J 2009 *Biomaterials* **30** 266–75
[4] Dahms S, Piechota H, Dahiya R, Lue T and Tanagho E 1998 *Br. J. Urol.* **82** 411–19
[5] Brown A, Farhat W, Merguerian P, Wilson G, Khoury A and Woodhouse K 2002 *Biomaterials* **23** 2179–90
[6] Cartwright L M, Shou Z, Yeger H and Farhat W A 2006 *J. Biomed. Mater. Res.* A **77** 180–4
[7] Badylak S F and Gilbert T W 2008 Immune response to biologic scaffold materials *Seminars in Immunology* vol 20 (Amsterdam: Elsevier) pp 109–16
[8] Pokrywczynska M, Gubanska I, Drewa G and Drewa T 2015 *Biomed. Res. Int.* **2015** 613439
[9] Bolland F, Korossis S, Wilshaw S P, Ingham E, Fisher J, Kearney J N and Southgate J 2007 *Biomaterials* **28** 1061–70
[10] Van Der Rest M and Garrone R 1991 *FASEB J.* **5** 2814–23
[11] Badylak S F 2004 *Transplant Immunol.* **12** 367–77
[12] Chen F, Yoo J J and Atala A 1999 *Urology* **54** 407–10
[13] Badylak S, Meurling S, Chen M, Spievack A and Simmons-Byrd A 2000 *J. Pediatr. Surg.* **35** 1097–103
[14] Rosario D J, Reilly G C, Ali Salah E, Glover M, Bullock A J and MacNeil S 2008 *Regen. Med.* **3** 145–56
[15] Keane T J, Swinehart I T and Badylak S F 2015 *Methods* **84** 25–34
[16] Schäfer F M and Stehr M 2018 *Innov. Surg. Sci.* **3** 107–18
[17] Morgante D, Radford A R, Abbas S, Ingham E, Subramaniam R and Southgate J 2021 *J. Tissue Eng.* **12** 2041731421998840

[18] Booth C, Korossis S A, Wilcox H E, Watterson K G, Kearney J N, Fisher J and Ingham E 2002 *J. Heart Valve Dis.* **11** 457–62
[19] Badylak S F, Tullius R, Kokini K, Shelbourne K D, Klootwyk T, Voytik S L, Kraine M R and Simmons C 1995 *J. Biomed. Mater. Res.* **29** 977–85
[20] Korossis S A, Wilcox H E, Watterson K G, Kearney J N, Ingham E and Fisher J 2005 *J. Heart Valve Dis.* **14** 408–21
[21] Lun S *et al* 2010 *Biomaterials* **31** 4517–29
[22] Freytes D O, Badylak S F, Webster T J, Geddes L A and Rundell A E 2004 *Biomaterials* **25** 2353–61
[23] Badylak S F, Lantz G C, Coffey A and Geddes L A 1989 *J. Surg. Res.* **47** 74–80
[24] Davis N, Callanan A, McGuire B, Mooney R, Flood H and McGloughlin T 2011 *J. Mech. Behav. Biomed. Mater.* **4** 375–82
[25] Crapo P M, Gilbert T W and Badylak S F 2011 *Biomaterials* **32** 3233–43
[26] Zhao F, Vaughan T J and Mcnamara L M 2015 *Biomechan. Model. Mechanobiol.* **14** 231–43
[27] Cooney G M, Lake S P, Thompson D M, Castile R M, Winter D C and Simms C K 2016 *J. Mech. Behav. Biomed. Mater.* **63** 134–40
[28] Shahmansouri N, Alreshidan M, Emmott A, Lachapelle K, Cartier R, Leask R L and Mongrain R 2016 *J. Mech. Behav. Biomed. Mater.* **64** 262–71
[29] Amini Khoiy K and Amini R 2016 *J. Biomech. Eng.* **138**
[30] Macrae R A, Miller K and Doyle B J 2016 *Strain* **52** 380–99
[31] Eilaghi A, Flanagan J G, Brodland G W and Ethier C R 2009 *J. Biomech. Eng.* **131** 091003
[32] Grassl E D, Barocas V H and Bischof J C 2004 Effects of freezing on the mechanical properties of blood vessels *ASME Int. Mechanical Engineering Congress and Exposition* vol 4711 pp 699–703